

Effect of Fines on Behavior of Braced Excavation in Sand: Experimental and Numerical Study

Subha Sankar Chowdhury¹; Kousik Deb²; and Aniruddha Sengupta³

Abstract: In this paper, the effect of fine content in the retained sandy soil on the behavior of braced excavation has been studied using experimental and numerical models in terms of four design factors: strut force, bending moment developed in the wall, lateral deflection of the wall, and vertical displacement of the ground surface. In the experiments, the fine content of the soil has been estimated as 0, 5, and 10% (by weight). However, the numerical study has been conducted for different fine contents varying from 0 to 50% (by weight). The parametric study with 20 m depth of retaining wall; position of struts at 2, 7, 12, and 17 m below ground level; wall thickness and embedment depth as 6 and 80% of depth of excavation; and stiffness of support members as 5×10^5 kN/m/m confirms that the values of the four design factors (strut force, wall moment, lateral wall deflection, ground deflection, and net earth pressure acting on the wall) increase with the increase in fine content in the retained soil. It is also observed that predominant ground surface displacement gradually shifts from heaving to settlement as the fine content in the retained soil increases. DOI: 10.1061/(ASCE)GM.1943-5622.0000487. © 2015 American Society of Civil Engineers.

Author keywords: Experimental modeling; Numerical modeling; Sand; Fines; Wall moment; Lateral wall movement; Vertical ground displacement.

Introduction

The construction of underground structures such as tunnels, water pipeline networks, or basements at a substantial depth below ground level in a congested urban area needs deep excavation with retaining wall and support system (struts), commonly known as braced excavation or propped retaining walls. Numerous works have been done to investigate the behavior of strutted retaining walls embedded within the ground on the basis of numerical modeling (Clough and Hansen 1981; Ng et al. 1995; Hashash and Whittle 1996; Vaziri 1996; Bose and Som 1998; Grande 1998; Hashash and Whittle 2002; Karlsrud and Andresen 2005; Costa et al. 2007; Hsiung 2009; Kung 2009). Although numerical models have been widely used to study the behavior of strutted excavation, physical modeling is also required to validate the results obtained from numerical study.

Physical or experimental models have been used in the past to assess complex geotechnical systems such as embedded supported retaining structures whose response is highly dependent on construction techniques, nonlinear soil–structure interactions, and variable geometries. Two-dimensional model tests and finite-element analysis for excavation problems in sand were performed by Nakai et al. (1999), and it was found that the surface displacement

of the backfill and earth pressure on the wall depend on the deflection of the wall. Furthermore, on the basis of the test results, it was concluded that wall friction, wall stiffness, and position and stiffness of strut significantly affect the earth pressure on the wall and the ground movement nearby the excavation. Centrifuge model tests of a vertical excavation in normally consolidated soft clay were carried out by Takemura et al. (1999), and the construction sequence of a doubly propped wall was properly simulated in the test. It was found that only 1 m embedment into the bottom sand can increase the stability of the excavation significantly and the deformation after a certain excavation depth is mainly dependent on stiffness of the sand. Moreover, it was also concluded that propping can prevent marked increment in the ground displacement. A large-scale model test was performed by Tefera et al. (2006) to study the excavation-induced wall deflection and ground displacement in relatively loose, dry sand, and the results were compared with that obtained from the numerical analysis. It has been observed that there is discrepancy between the two results, and on the basis of this discrepancy, improved procedure for parameter estimation regarding numerical simulation has been suggested. A number of physical model tests on braced excavation were performed by Bryson and Zapata-Medina (2007) to investigate the behavior of excavation support systems and the associated ground deformations. The model test results were compared with both state-of-the-art practice ground deformation prediction methodologies and field observations. It has been shown that scale model test data can be reliably extrapolated to equivalent prototype data to evaluate excavation support system behavior and soil response associated with deep excavations.

In most of the previous experimental works done on strutted excavation, the retained soil was either cohesionless or cohesive in nature. However, under actual field conditions, fines may be present in the sandy soil retained by the wall. Thus, it is required to study the effect of fines present in sand on the behavior of the braced excavation. The effect of gradual increase of fine content in the sand should also be studied. In the present work, the behavior of a propped retaining wall under mixed soil conditions (different

¹Research Scholar, Dept. of Civil Engineering, Indian Institute of Technology Kharagpur, Kharagpur 721302, India. E-mail: chowdhurysubha@gmail.com

²Associate Professor, Dept. of Civil Engineering, Indian Institute of Technology Kharagpur, Kharagpur 721302, India (corresponding author). E-mail: kousik@civil.iitkgp.ernet.in

³Professor, Dept. of Civil Engineering, Indian Institute of Technology Kharagpur, Kharagpur 721302, India. E-mail: sengupta@civil.iitkgp.ernet.in

Note. This manuscript was submitted on April 17, 2014; approved on December 18, 2014; published online on May 2, 2015. Discussion period open until October 2, 2015; separate discussions must be submitted for individual papers. This paper is part of the *International Journal of Geomechanics*, © ASCE, ISSN 1532-3641/04015018(13)/\$25.00.

percentage of fines with sand) has been investigated with the help of both physical as well as numerical modeling in terms of the four design factors, i.e., strut load, wall deflection, wall moment, and ground surface displacements measured at different stages of the excavation. The experimental results are compared with those obtained from numerical analysis using finite-difference-based software *FLAC-2D* (Itasca 2005). The experiments have been done for 0, 5, and 10% fine contents by weight, whereas numerical analysis is done for 0, 5, 10, 20, 30, 40, and 50% fine content by weight. Only one-half of the strutted excavation problem has been modeled in the laboratory. The half-width of the excavation ($B/2$) has been taken as 0.25 m in the physical model. The depth of the wall (D), depth of excavation (D_e), and embedment depth of the wall (D_b) have been taken as 1, 0.5, and 0.5 m, respectively, in the physical model. The depth of the strut below ground level has been chosen as 0.15 m. Parametric study has been done for a prototype structure with depth of excavation as 20 m and considering four levels of struts.

Physical Model

Model Tank

The model tank used in the experiment was 1.4×1.4 m in plan with a height of 1.33 m. The overall view of the tank, removable segments, lowermost fixed portions, and the whole model with wall and strut are shown in Figs. 1(a–d), respectively. One of the sides of the tank was made of transparent plexiglass, and the other three sides were made up of steel plates. One-half of the excavation was modeled in the experiment. The centerline of excavation was coincident with one face of the tank and that face was made

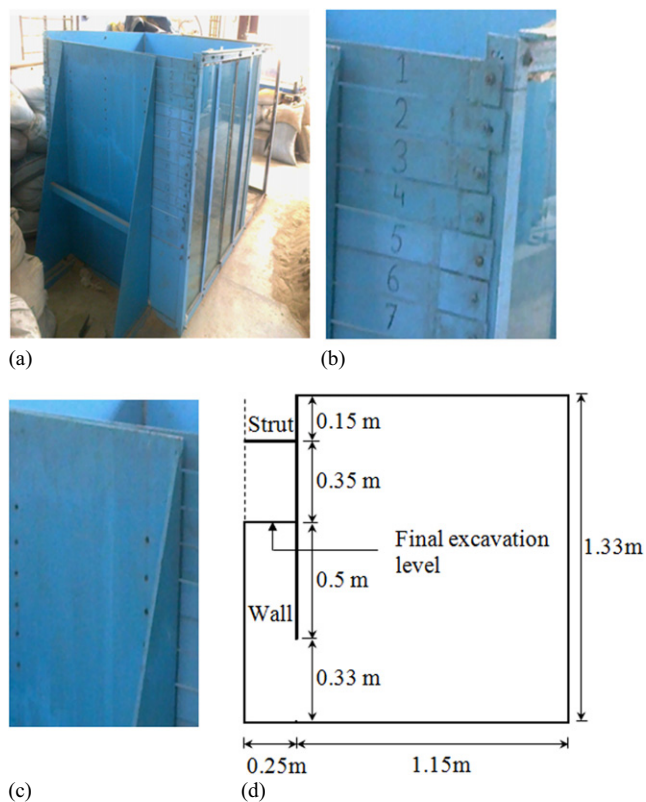


Fig. 1. Model test tank constructed in laboratory with (a) overall view; (b) removable segments; (c) fixed plate where struts are attached at one end; and (d) schematic diagram showing retaining wall and strut

up of removable metallic strips. Initially, during the filling of the tank, these removable metallic strips were kept in place on that side. The strips were removed sequentially when the soil in front of the wall was required to be excavated at different stages.

Model Structures (Wall, Struts, and Waler Beams)

The model wall was made up of a plexiglass sheet of 6 mm thickness and 1 m height spanning the width (1.4 m) of the tank. The half-width of the excavation was taken as 0.25 m, so the wall was placed at a distance of 0.25 m from the centerline. Two struts were spaced at a horizontal spacing of 0.7 m. The length of the each strut was 0.25 m with a cross-sectional dimension of 0.0165×0.0165 m. The location of the struts was 0.15 m below the top of the ground surface. Both wall and struts were made up of plexiglass material (density, Young's modulus, and Poisson's ratio are $1,250 \text{ kg/m}^3$, $6,333 \text{ MPa}$, and 0.15 , respectively). The Young's modulus and Poisson's ratio were determined from a tensile test in which one end of a rectangular bar of plexiglass was kept fixed and the other end was pulled with a force. The lateral (perpendicular to the direction of loading) and longitudinal (along the direction of loading) strains were measured with strain gauges attached on the material surface. The Young's modulus was calculated from the stress–strain data. Similarly, Poisson's ratio was calculated from lateral and longitudinal strain data. A rectangular beam of the same material with cross-sectional dimension of 0.05×0.01 m was used as a waler beam, with which the struts were connected to the wall. The length of the waler beam was 1.38 m and placed along the width of the model wall. Holes were provided at the two ends of the struts and also on the wall at the predetermined locations of the struts. The bolts were glued to the wall through the holes. The struts were connected to the wall with the help of these bolts coming out of the walls. The other end of the struts was free to move vertically along a groove within a rigid plate located at the centerline of the excavation (as shown in Fig. 2). The properties of model structures are presented in Table 1. In Table 1, the flexural rigidity of the model wall and the stiffness of the model struts are calculated as $E_{\text{wall}}I_{\text{wall}}$ and $A_{\text{strut}}E_{\text{strut}}/ls$, where E_{wall} , I_{wall} , A_{strut} , E_{strut} , l , and s are modulus of elasticity of the wall material, moment of inertia per unit length of the wall, cross-sectional area of a strut, modulus of elasticity of strut material, length of strut, and horizontal spacing of strut, respectively. The half-width of excavation (B') was kept as 0.25 m in the model tank, and the distance between toe of the wall and the bottom of the model tank (y) was kept as 0.33 m, so that $B'/y = 1.33$ in the experiment. This is in accordance with the tests done by other researchers [$B'/y = 1.33$ per Nakai et al. (1999) and $B'/y = 2.0$ per Tefera et al. (2006)].

Soil Conditions

The experiment was done with three different fill materials: (1) 100% sand; (2) 5% fines mixed with sand; and (3) 10% fines mixed with sand. The shear strength parameters and interface properties (between soil and wall) for all the sandy soils mixed with 0, 5, 10, 20, 30, 40, and 50% fines were obtained from laboratory tests. For all the model tests, the bulk unit weight and the moisture content of the soil were kept as 16 kN/m^3 and 10%, respectively. The cohesion, friction angle, and modulus of elasticity of the soils were obtained from triaxial tests, and the interface friction angle and adhesion between wall and soil were obtained from direct shear tests. In the direct shear test, a plexiglass block was placed into the lower half of the direct shear box, and the upper half of the box was filled with sand (with and without fines). In the numerical

analyses, the value of the friction angle from the triaxial tests has been increased by 10% to obtain the values under plane-strain conditions (Wroth 1984). The properties of the pure sand and fines are shown in Tables 2 and 3, respectively. The properties of the retained soil and interface properties between wall and soil mixed with different percentages of fines are given in Table 4. The test tank was initially filled with the soil by compacting it in different layers (each 100 mm in thickness), maintaining the uniform bulk unit weight and moisture content. In the numerical analyses, the value of the coefficient of earth pressure at rest (K_0) has been assumed as $1 - \sin \phi$, where ϕ = friction angle of soil under plane-strain conditions. The value of Poisson's ratio for soil (μ) is calculated from $\mu = K_0/(1 - K_0)$.

Experimental Procedure

Initially, the test tank was filled to a height of 0.33 m from the bottom. Before filling the tank, silica gel was used on the side wall surfaces to reduce the friction. The model wall was inserted from the top of the tank with the help of a support. After insertion of the model wall in the tank, the remaining volume of the tank was filled

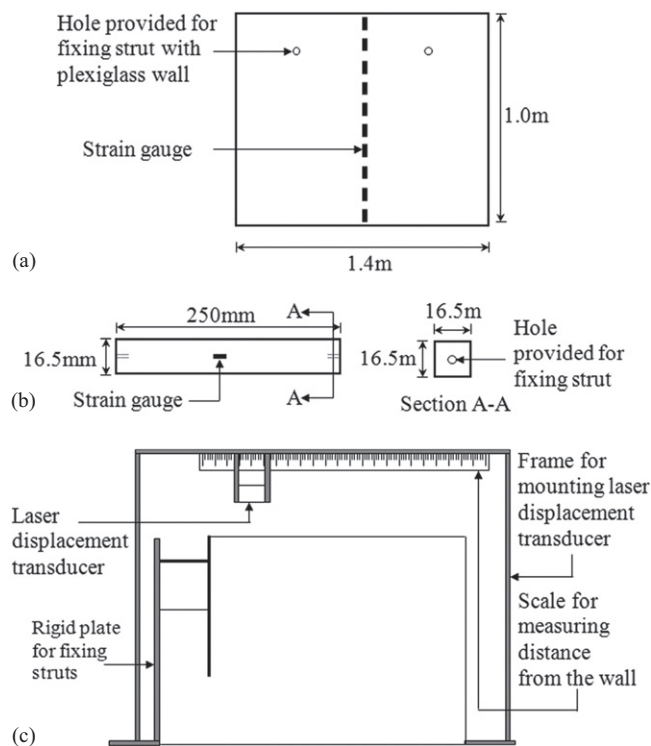


Fig. 2. Schematic diagram showing instrumentation with (a) strain gauges on model retaining wall; (b) strain gauges on both surfaces of strut; and (c) laser-displacement transducer

up with soil, and the top surface of the soil was flush with the top of the wall.

After filling the tank and installing the wall, the different construction stages followed in the experiment are as follows:

- First stage: Removal of soil from the front side of the wall up to a depth of 0.15 m below the top.
- Second stage: Installation of water beam and struts at 0.15 m below the top. The water beam was placed along the width of the tank. Two struts were installed at a horizontal spacing of 0.7 m from each other. One end of the struts was connected to the wall, and the other end was connected to the plate located along the centerline of excavation.
- Third stage: Removal of soil up to a depth of 0.5 m below the top of the wall.

Table 1. Properties of Model Structures Used in the Analysis

Properties	Wall	Strut
Modulus of elasticity (MPa)	6,333	6,333
Thickness (m)	0.006	—
Length (m)	1	0.25
Cross-sectional area (m ²)	0.006	2.7225×10^{-4}
Horizontal spacing (m)	—	0.7
Flexural rigidity of wall (N · m ² /m)	114	—
Stiffness of struts (N/m/m)	—	9.85×10^6

Table 2. Properties of Sand Used in Experiment

Properties	Values
Sand	100%
Silt-clay fraction	0%
Coefficient of uniformity, C_u	2.5
Coefficient of curvature, C_c	0.9
Specific gravity	2.72
Minimum dry unit weight, $\gamma_{d, \min}$	14 kN/m ³
Maximum dry unit weight, $\gamma_{d, \max}$	18 kN/m ³
Minimum void ratio, e_{\min}	0.54
Maximum void ratio, e_{\max}	0.88

Table 3. Properties of Fines Used in Experiment

Properties	Values
Sand	8%
Silt	68%
Clay	24%
Liquid limit	51%
Plastic limit	19%
Plasticity index	32%
Specific gravity	2.67
Optimum moisture content	20%
Minimum dry unit weight, $\gamma_{d, \max}$	18 kN/m ³

Table 4. Properties of Soil and Interface Used in Numerical Analysis for Model and Prototype Structures

Fine (%)	Soil			Interface		Model parameters for Eq. (1)	
	c (kN/m ²)	ϕ (degrees)	μ	c_a (kN/m ²)	δ (degrees)	k	n
0	0	32	0.30	0	25	133.55	0.45
5	7.3	29	0.32	0.5	22	120.57	0.49
10	22.6	24	0.36	2.9	19	106.46	0.52
20	33.2	20	0.39	3.6	17	82.92	0.55
30	43.8	17	0.40	3.9	16	62.93	0.58
40	49.4	12	0.44	5.2	12	53.12	0.70
50	51.0	10	0.45	6.5	10	47.07	0.74

Instrumentations

The instrumentations of the model retaining wall, strut, and top surface are shown in Figs. 2(a–c), respectively. Before installing the model wall, strain gauges were attached onto the model wall (as shown in Fig. 3). The strain gauges were located along the centerline of the model wall to avoid the boundary effect of the tank on the two sides. The topmost and bottommost strain gauges were located at the top and the toe of the wall, respectively. The locations of the other strain gauges were 0.1, 0.2, 0.3, 0.4, 0.5, 0.6, 0.7, 0.8, and 0.9 m below the top of the wall. The strain gauges were also attached on two opposite surfaces of the struts. The strain gauges were used to measure the strains experienced by the wall and the struts at different stages of the excavation. From these strain data, the bending moment and the lateral deflection of the wall were calculated. A laser displacement transducer was used to estimate the displacement of the top ground surface during different stages of the braced excavation construction. For all the stages of the strutted excavation, the strains in the wall and the struts and the ground surface displacements were measured.

Numerical Simulation

The numerical analysis of the propped retaining wall has been done using commercially available software, *FLAC-2D*, which is based on the finite-difference method. The problem is considered as a two-dimensional plane-strain problem with centerline of symmetry of the excavation coinciding with the one end of the model boundary. The soil is modeled as a linearly elastic-perfectly plastic material following Mohr–Coulomb failure criterion. The modulus of elasticity of soil has been calculated from the following hyperbolic relation as suggested by Janbu (1963) (see Hatami and Bathurst 2005, 2006) for elastic-plastic soil as

$$E_i = KP_a \left(\frac{\sigma_3}{P_a} \right)^n \quad (1)$$

where K = modulus number; n = modulus exponent; P_a = atmospheric pressure (taken as 101.325 kN/m²); and σ_3 = confining pressure. The triaxial tests have been done for three different confining pressures. For each confining pressure from triaxial tests, one E_i value is obtained. The values of the parameters n and K are obtained from triaxial test results. Once the values of n and K are determined, the value of E_i is varied

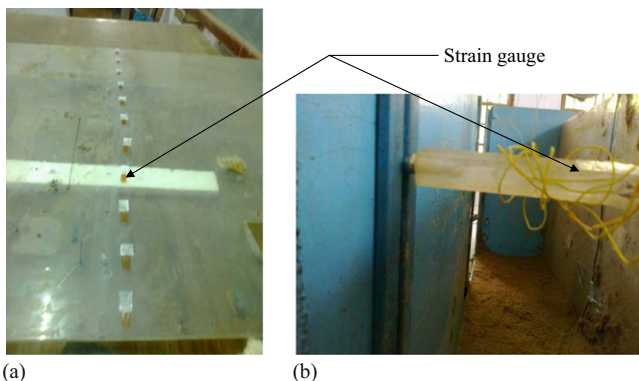


Fig. 3. Strain gauges attached to the plexiglass: (a) retaining wall; (b) strut

according to Eq. (2) in the numerical model. The bulk modulus (K) and shear modulus (G) are also varied according to the following equations:

$$G = \frac{E_i}{2(1 + \mu)} \quad (2)$$

$$K = \frac{E_i}{3(1 - 2\mu)} \quad (3)$$

where μ = Poisson's ratio of soil.

The interface parameters between wall and soil, i.e., friction angle (δ) and cohesion (c_a), are estimated from the direct shear test results. The interface normal and shear stiffness (K_n and K_s) are estimated from bulk modulus, shear modulus of the soil within the depth of the wall, and the width of the zone normal to the wall. The interface normal and shear stiffness are given by

$$K_n = K_s = 10 \times \frac{(K + \frac{4}{3}G)}{\Delta z_{\min}} \quad (4)$$

where Δz_{\min} = smallest width of an adjoining zone in the normal direction to the interface. The values of K_n and K_s are calculated when G and K reach their maximum values, i.e., at the centroid of mesh adjacent to the toe of the retaining wall.

The numerical model shown in Fig. 4 is developed for validating the experimental results. The uniform zone size in the numerical analysis of model structures is kept as 0.05 m. Thus, the height of the numerical model is kept as 1.35 m. However, 1.33 m is the height of the tank used in the laboratory. The boundary condition in the numerical model is such that the nodes along the bottom boundary of the model are fixed in both horizontal as well as vertical directions, whereas the nodes along the two vertical boundaries are restrained against movement along horizontal directions only. For the analysis of a real-life structure in which the depth of excavation is 20 m, the zone size is kept as 1 m, and the total number of zones and nodes are 4,860 and 5,002, respectively.

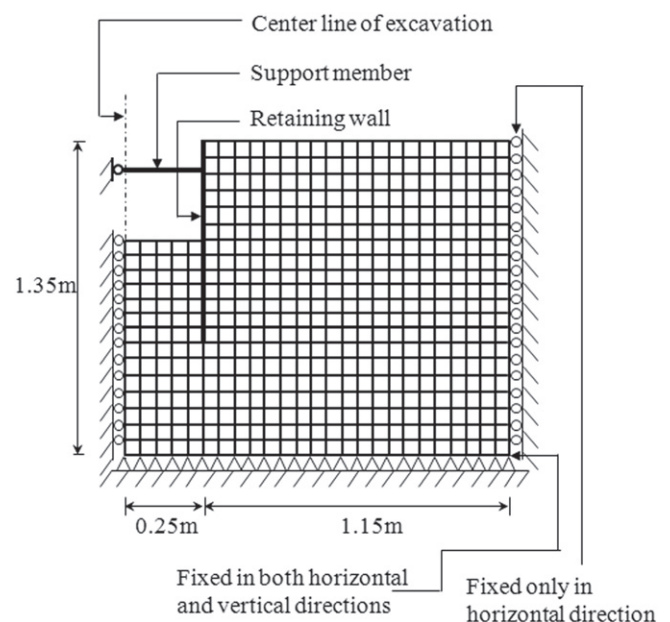


Fig. 4. Numerical model used for validation with experimental data

Results and Discussion

Comparison between Results Obtained from Experiment and Numerical Study

The data from the strain gauges on the wall are used to calculate the bending moment developed in the wall and lateral deflection of the wall (a typical set of strain gauge data is presented in Table 5, which indicates the strain change of the retaining wall due to excavation effect). Initially, the curvature is calculated from the strain values (strain value is the difference between the final and initial value, as shown in Table 5). Then the curvature data along different heights of the wall are fitted with a polynomial curve, and the equation is integrated to obtain the deflection of the wall. The bending moments at different depths from the top of the wall are calculated by multiplying the curvature values with flexural rigidity ($E_{\text{wall}}I_{\text{wall}}$) of the wall, where E_{wall} = modulus of elasticity of wall material and I_{wall} = moment of inertia of wall section considering unit length along the excavation. The calculation of lateral displacement from strain is based on the assumption of elasticity of the retaining wall. If the retaining wall yields, this calculation from strain to lateral displacement may not be reasonable. However, the maximum strain as calculated from strain gauge data is 4.35×10^{-3} or 0.435% (among all the tests), and from the stress-strain curve of the wall material it is revealed that stress increases with strain linearly even beyond a strain value of 0.5%, which is greater than 0.435%. Thus, it can be said that the yield stress of the material is not reached for the deflection of the

Table 5. Typical Strain Data for Retaining Wall Measured during Test

Depth of strain gauge below top of the wall (m)	Strain values ($\times 10^{-6}$) at different stages	
	After installation of wall	After excavation up to 0.5 m from top
0.00	-11,768	-16,120
0.10	-731	-559
0.20	4,620	3,421
0.30	13,816	13,658
0.40	40,297	40,450
0.50	16,961	17,025
0.60	8,653	8,680
0.70	1,386	1,408
0.80	21,552	21,590
0.90	983	1,001
1.00	17,892	17,916

Table 6. Typical Strain Data for Strut Measured during Test

Strain values ($\times 10^{-6}$) at different stages	
After installation of strut at 0.15 m below top	After excavation up to 0.5 m from top
19,557	19,499
1,112	1,045

Table 7. Comparison of Strut Force and Wall Bending Moment from Experiment and Numerical Study for Different Fine Contents when $D_e = 0.5$ m

Fine content in soil (%)	Nondimensional strut force ($F^* = F/\gamma D_e^2$) (%)			Maximum nondimensional moment in wall ($M^* = M/\gamma D_e^3$) (%)		
	Experimental model	Numerical model	Difference (%)	Experimental model	Numerical model	Difference (%)
0	7.94	7.47	6	0.55	0.56	2
5	3.85	3.77	2	0.19	0.17	11
10	4.28	4.40	3	0.29	0.25	14

wall as encountered in the experiment. The data obtained from strain gauges (as presented in Table 6) that are attached to the strut are used to calculate the axial load carried by the strut. If the strain is ϵ , then axial load is calculated as $F = \epsilon A_{\text{strut}} E_{\text{strut}}$, where A_{strut} = cross-sectional area of the strut and E_{strut} = Young's modulus of the strut material. The ground surface displacement is measured by laser-type displacement transducer. The values of axial force carried by the struts, the bending moment developed in the wall, the deflection of the wall, and the ground surface displacement are calculated corresponding to each stage of the excavation and also for different backfill soils.

Strut Force

The force acting in the model strut at the third stage (excavation up to 0.5 m below the top) is normalized with respect to γD_e^2 (where γ = bulk unit weight of soil taken as 16 kN/m³ and D_e = depth of excavation, i.e., 0.5 m), and the values of $F^* = F/\gamma D_e^2$ (expressed as percentage) as obtained from experiment and numerical study for different percentage of fine contents are presented in Table 7. It can be found from Table 7 that the value of F^* decreases by 52 and 50% when fine content increases from 0 to 5% for the experimental and numerical study, respectively. However, the value of F^* increases by 11 and 14% when fine content increases from 5 to 10% for the experimental and numerical study, respectively. It is also observed that the overall difference in the values of nondimensional strut force between experimental and numerical model is around 2–6%.

Wall Moment

The bending moment in the model wall is normalized with respect to γD_e^3 ($M^* = M/\gamma D_e^3$). The distribution of M^* (at the third stage of excavation) along the depth of the wall for fine contents of 0, 5, and 10% is shown in Figs. 5(a–c), respectively. The maximum wall moment at the third stage is presented in Table 7 for fine contents of 0, 5, and 10%. It can be seen from Table 7 that the value of nondimensional moment M^* decreases by 65 and 70% when fine content increases from 0 to 5% for the experimental and numerical model, respectively. However, it increases by 53 and 47% in the experimental model and numerical model, respectively, when fine content increases from 5 to 10%. Moreover, for fine contents of 0, 5, and 10%, the value of M^* as obtained numerically is 2% higher, 11% lower, and 14% lower than that obtained by the experimental study. From the results, it can be said that the difference between the nondimensional wall moment in the experimental and numerical models is in the range of (2–14%).

Wall Deflection

The value of the lateral wall deflection during the third stage of the excavation as obtained from experiment and numerical modeling for different percentage of fine content is normalized with respect to depth of excavation, D_e ($u^* = u/D_e$). The maximum nondimensional lateral wall deflection is presented in Table 8, and the distribution of u^* (at the third stage of excavation) along the depth of the wall for fine contents of 0, 5, and 10% is shown in

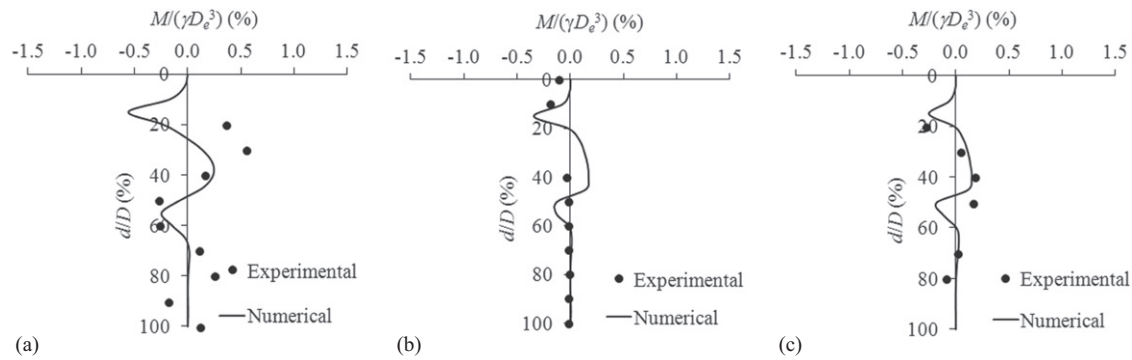


Fig. 5. Comparison of the distribution of nondimensional wall moment from experiment and numerical analysis for fine contents of (a) 0; (b) 5; and (c) 10%

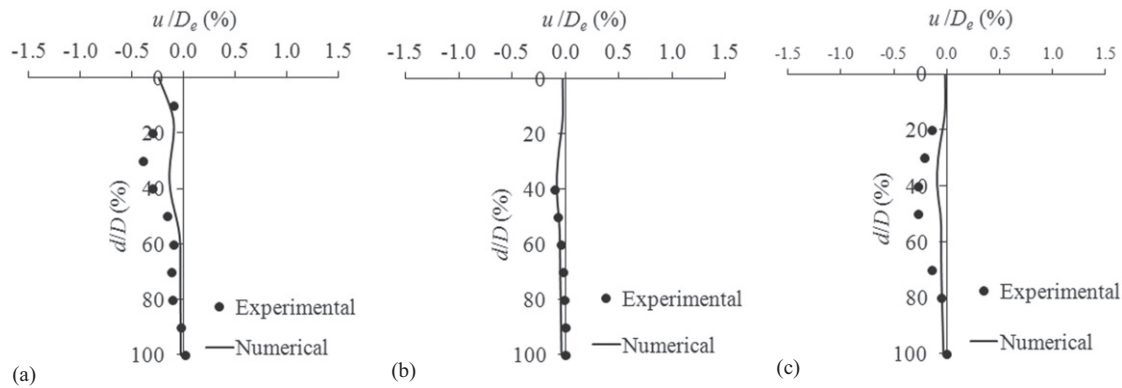


Fig. 6. Comparison of distribution of nondimensional wall deflection from experiment and numerical analysis for fine contents of (a) 0; (b) 5; and (c) 10%

Table 8. Comparison of Wall Deflection and Ground Surface Displacement from Experimental and Numerical Study for Different Fine Contents when $D_e = 0.5$ m

Fine content in soil (%)	Maximum nondimensional wall deflection ($u^* = u/D_e$) (%)			Maximum nondimensional ground surface displacement ($v^* = v/D_e$) (%)		
	Experimental model	Numerical model	Difference (%)	Experimental model	Numerical model	Difference (%)
0	0.41	0.25	39	0.24	0.25	4
5	0.10	0.08	20	0.06	0.08	33
10	0.27	0.09	67	0.11	0.10	9

Figs. 6(a–c), respectively. Table 8 shows that the value of u^* decreases by 76 and 68% when fine content increases from 0 to 5% for the experimental and numerical models, respectively. However, the value of u^* increases by 170 and 12.5% when the fine content increases from 5 to 10% for the experimental and numerical models, respectively. Furthermore, it has been found that the value of maximum nondimensional wall deflection as obtained by numerical modeling is 39, 20, and 67% lower than the values measured from the tests when fine contents are 0, 5, and 10%, respectively. From the preceding discussion, it can be said that the variation of nondimensional wall deflection between the experimental and numerical models is in the range of (20–67%). This may be because of the fact that in the numerical modeling, the interface model properties are determined according to the guidelines provided by *FLAC*. The interface properties may not accurately represent the actual interface behavior. To determine the actual interface properties by experiment is also very difficult. The use of the Mohr–Coulomb model, although much accepted in geotechnical engineering, has some approximations in modeling such complicated soil–structure interaction problems as the present one.

Ground Surface Displacement

The displacement of the ground surface (v) adjacent to the strutted excavation during the third stage of the excavation as obtained from experiment and numerical modeling for different percentage of fine content is normalized with respect to depth of excavation, D_e (i.e., $v^* = v/D_e$). The distribution of nondimensional ground surface displacement, v^* (at the third stage of excavation), for both the experimental and numerical models along the normalized distance from the wall, i.e., x/D , where x = distance from the wall and D = depth of wall, is shown in Figs. 7(a–c) for fine contents of 0, 5, and 10%, respectively. The maximum nondimensional ground displacement is presented in Table 8. It can be found from Table 8 that the value of normalized ground surface displacement, v^* , decreases by 75 and 68% when fine content increases from 0 to 5% for the experimental and numerical models, respectively. Furthermore, the value of v^* increases by 83 and 25% when fine content increases from 5 to 10% for the experimental and numerical models, respectively. Furthermore, it has been found that value of v^* as obtained by numerical modeling is 4% higher, 33% higher, and 9% lower than the values measured from the tests

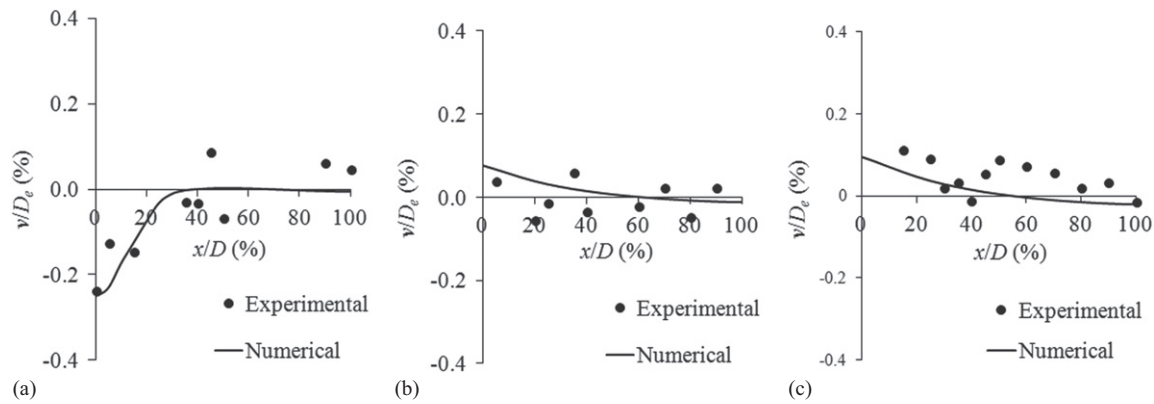


Fig. 7. Comparison of distribution of nondimensional ground surface displacement from experiment and numerical analysis for fine contents of (a) 0; (b) 5; and (c) 10%

Table 9. Effect of Fines on Normalized Strut Force F^* when D_b/D_e Varies from 60 to 120%

$F^* = F/\gamma D_e^2$ (%)	D_b (m)	D_b/D_e (%)	t_{wall}/D_e (%)	$k_{\text{strut}} \times 10^5$ (kN/m/m)	Fines (%)						
					0	5	10	20	30	40	50
First-level strut	12	60	6	5	22.45	26.69	33.89	40.61	45.39	56.55	61.59
	16	80	6	5	23.20	27.45	34.38	41.30	46.20	57.33	62.47
	20	100	6	5	24.14	28.28	35.14	42.11	46.86	58.06	63.56
	24	120	6	5	24.88	29.42	36.02	43.13	48.03	59.41	62.56
Second-level strut	12	60	6	5	80.83	91.61	108.88	130.91	148.66	175.47	187.81
	16	80	6	5	82.66	93.14	110.64	132.94	150.61	178.13	190.78
	20	100	6	5	85.67	95.42	111.67	134.59	152.69	179.53	191.72
	24	120	6	5	87.77	96.38	114.06	136.20	154.47	181.88	192.66
Third-level strut	12	60	6	5	91.77	101.58	119.47	140.75	156.22	182.66	195.31
	16	80	6	5	92.28	102.36	121.73	143.38	159.53	186.41	197.97
	20	100	6	5	92.73	103.45	123.95	145.77	162.81	189.69	201.09
	24	120	6	5	94.73	105.75	125.22	147.25	164.69	191.09	203.28
Fourth-level strut	12	60	6	5	41.34	44.92	55.05	63.66	70.17	90.25	98.38
	16	80	6	5	41.88	45.91	55.83	65.06	70.94	89.75	99.16
	20	100	6	5	42.86	46.92	56.80	66.19	72.30	89.97	99.38
	24	120	6	5	43.45	47.50	57.84	67.56	73.52	90.06	98.19

when fine contents are 0, 5, and 10%, respectively. The variability of the ground surface displacement in the experiments is due to the fact that near the wall, the measurement of deformation is more accurate compared with the measurements away from the wall. This is due to the fact that near the wall, the ground surface has a measurable amount of deformation, and as one goes away from the wall, the ground surface deformation becomes smaller and smaller, and the accuracy of measurement decreases. From the preceding discussion, it can be said that the variation of nondimensional ground surface displacement between the experimental and numerical models is in the range of (4–33%). Thus, the results obtained from the experimental and numerical study are very comparable.

Parametric Study

Parametric study has been done using numerical modeling by varying the fine content of the retained soil through 0, 5, 10, 20, 30, 40, and 50%. A real-life braced retaining structure is considered where the depth of excavation is taken as 20 m. The modulus of elasticity and Poisson's ratio of reinforced concrete wall are taken as 2.96×10^{10} Pa and 0.15, respectively. In the parametric study, the arrangement of the strut is fixed per the recommendations reported by Chowdhury et al. (2013), i.e., at 2, 7, 12, and 17 m below ground level, respectively. The other design

parameters, i.e., thickness of wall, stiffness of struts, and embedment depth are varied in the range (4–10)% of D_e , $(1-125) \times 10^5$ kN/m/m, and 60–120% of D_e , respectively, including the design recommendations given in Chowdhury et al. (2013). For the variation of each design factor, the other two are kept at their optimum values, i.e., 5×10^5 kN/m/m and 80% of D_e , 6% of D_e and 80% of D_e , and 6% of D_e and 5×10^5 kN/m/m, respectively.

Effect of Fines on Strut Force

In the numerical analysis of the prototype structure, the maximum forces (F) coming in the struts at the four levels are normalized with respect to γD_e^2 , and the variation of $F^* = F/\gamma D_e^2$ (expressed in percentage) with different fine contents is shown in Tables 9–11 when D_b/D_e varies from 60% to 120%, t_{wall}/D_e varies from 4 to 10%, and k_{strut} varies from 1×10^5 to 125×10^5 kN/m/m. It is observed that for a particular value of D_b/D_e , t_{wall}/D_e , and k_{strut} , the strut force (F^*) increases owing to the addition of fines. However, in most of the cases, the rate of increment decreases beyond the fine content of 40% at all four levels of strut. The maximum variation of F^* at the first-level, second-level, third-level, and fourth-level struts is 174, 132, 117, and 138% for the variation of fine content from 0 to 50%. It is further observed that for a particular fine content, the value of F^* increases with increase in D_b/D_e , except when fine content is 50%, where it decreases for

Table 10. Effect of Fines on Normalized Strut Force F^* when t_{wall}/D_e Varies from 4 to 10%

$F^* = F/\gamma D_e^2$ (%)	D_b/D_e (%)	t_{wall} (mm)	t_{wall}/D_e (%)	$k_{\text{strut}} \times 10^5$ (kN/m/m)	Fines (%)						
					0	5	10	20	30	40	50
First-level strut	80	800	4	5	17.25	20.31	25.84	31.22	34.98	43.33	46.77
	80	1,200	6	5	23.20	27.45	34.38	41.30	46.20	57.33	62.47
	80	1,600	8	5	29.50	35.53	43.08	51.64	57.28	71.44	78.55
	80	2,000	10	5	37.91	45.59	53.89	62.97	65.67	85.72	94.00
Second-level strut	80	800	4	5	60.97	70.20	83.33	99.05	111.55	132.59	142.11
	80	1,200	6	5	82.66	93.14	110.64	132.94	150.61	178.13	190.78
	80	1,600	8	5	100.34	111.17	133.05	159.84	182.03	212.81	225.16
	80	2,000	10	5	113.72	123.23	146.63	179.06	203.75	235.16	247.66
Third-level strut	80	800	4	5	84.33	93.31	111.02	129.91	143.66	171.09	182.66
	80	1,200	6	5	92.28	102.36	121.73	143.38	159.53	186.41	197.97
	80	1,600	8	5	96.42	107.08	127.17	151.00	169.06	195.94	209.06
	80	2,000	10	5	103.64	111.11	136.50	160.78	179.06	207.03	224.22
Fourth-level strut	80	800	4	5	42.84	46.33	56.38	65.16	69.94	89.72	100.86
	80	1,200	6	5	41.88	45.91	55.83	65.06	70.94	89.75	99.16
	80	1,600	8	5	41.55	45.69	55.78	65.63	72.47	90.89	98.09
	80	2,000	10	5	41.89	45.47	56.27	66.72	75.36	93.39	99.81

Table 11. Effect of Fines on Normalized Strut Force F^* when k_{strut} Varies from 1×10^5 to 125×10^5 kN/m/m

$F^* = F/\gamma D_e^2$ (%)	D_b/D_e (%)	t_{wall}/D_e (%)	$k_{\text{strut}} \times 10^5$ (kN/m/m)	Fines (%)						
				0	5	10	20	30	40	50
First-level strut	80	6	1	21.89	26.13	32.73	39.66	44.58	55.38	60.56
	80	6	5	23.20	27.45	34.38	41.30	46.20	57.33	62.47
	80	6	25	25.22	29.66	36.58	43.52	48.23	59.36	64.69
	80	6	125	34.70	38.98	45.89	52.55	57.42	67.16	72.02
Second-level strut	80	6	1	64.89	72.59	86.19	102.28	115.61	136.38	145.83
	80	6	5	82.66	93.14	110.64	132.94	150.61	178.13	190.78
	80	6	25	97.83	108.33	127.50	152.22	171.41	201.25	214.84
	80	6	125	123.05	134.86	149.98	174.84	193.75	224.22	243.91
Third-level strut	80	6	1	69.77	77.14	92.33	108.31	119.83	141.95	151.16
	80	6	5	92.28	102.36	121.73	143.38	159.53	186.41	197.97
	80	6	25	116.31	128.44	153.17	179.84	199.53	234.22	250.63
	80	6	125	132.89	143.02	180.31	211.41	235.00	273.28	282.50
Fourth-level strut	80	6	1	28.67	31.27	38.39	44.72	48.95	62.45	70.67
	80	6	5	41.88	45.91	55.83	65.06	70.94	89.75	99.16
	80	6	25	51.69	56.47	69.11	81.06	88.89	112.22	121.64
	80	6	125	57.88	62.31	74.69	88.42	96.89	119.91	127.80

the first-level and fourth-level struts when D_b/D_e increases from 100 to 120%. For a particular fine content, the value of F^* at the first, second, and third levels increases with the increase in t_{wall}/D_e ; however, the value of F^* for the fourth-level strut decreases with the increase in t_{wall}/D_e when fine content is 50%. Furthermore, it has been found that for a particular fine content, the value of F^* at the first, second, and third levels increases with the increase in k_{strut} . This may be due to the fact that if the strut becomes stiffer, its ability to carry force increases. Thus, for a similar type of retained soil, a stiffer strut will attract more force as compared with other struts.

Table 9 shows that when D_b/D_e changes from 80 to 100%, the rate of increment of normalized axial force in the first-level, second-level, and fourth-level support members (or struts) gradually decreases for variation of fine content from 0 to 50%. From Table 11 it is observed that when k_{strut} varies from 5×10^5 to 25×10^5 kN/m/m, the rate of increment of normalized axial force in the first-level and second-level support members (or struts) also decreases for variation of fine content from 0 to 50%. However, a similar type of variation is obtained for the fourth-level strut when the stiffness of struts varies from 25×10^5

to 125×10^5 kN/m/m. Thus, it can be said that because of the increase in the depth of embedment and the stiffness of the strut, the strut force increases. However, the rate of increment decreases because of the increase in fines.

Effect of Fines on Wall Moment

The variations of normalized wall moment with normalized wall depth as obtained from numerical analyses of the prototype structure for different fine contents when $D_b/D_e = 80\%$, $t_{\text{wall}}/D_e = 6\%$, and $k_{\text{strut}} = 5 \times 10^5$ kN/m/m are shown in Fig. 8. The values of moment (M) are normalized with respect to γD_e^3 ($\gamma =$ unit weight of soil and $D_e =$ depth of excavation) and the normalized moment is calculated as $M^* = M/\gamma D_e^3$. The depth, z , below ground level is normalized with respect to total depth of wall, D . It is revealed from Fig. 8 that patterns of bending moment distribution along the depth of the wall and the location of maximum moment are similar for different fine contents. The variations of normalized maximum wall moment (expressed in percentage) with different fine contents when D_b/D_e varies from 60 to 120%, c varies from 4 to 10%, and k_{strut} varies from 1×10^5 – 125×10^5 kN/m/m are presented in Table 12. It is

observed from Table 12 that for a particular value of D_b/D_e , t_{wall}/D_e , and k_{strut} , the value of M^* increases with increase in fine content, but beyond fine content of 40%, the rate of increment of M^* reduces. Moreover, it can be found from Table 12 that the maximum variation of M^* is around 180% when fine content varies from 0 to 50%. For a particular fine content, the bending moment in the wall increases with increase in wall thickness because the moment of inertia of the wall increases with wall thickness, which in turn increases the flexural rigidity of the wall. Thus, it becomes more capable for carrying a higher moment. Furthermore, for a particular fine content, the value of M^* is maximum when $k_{strut} = 1 \times 10^5$ kN/m/m; it decreases at 5×10^5 kN/m/m and remains almost constant up to strut stiffness of 25×10^5 kN/m/m, beyond which it again increases. Thus, irrespective of fine content, the bending moment is lowest when the strut stiffness is kept in between $(5-25) \times 10^5$ kN/m/m. It can be also found from Table 12 that when t_{wall}/D_e varies from 6 to 8%, the rate of increment of normalized bending moment in the retaining wall increases from 36 to 44%, when fine content varies from 0 to 50%, respectively. Thus, it can be said that owing to the increase of thickness of the wall, the wall moment increases, and the rate of increment increases owing to the increase of fine content.

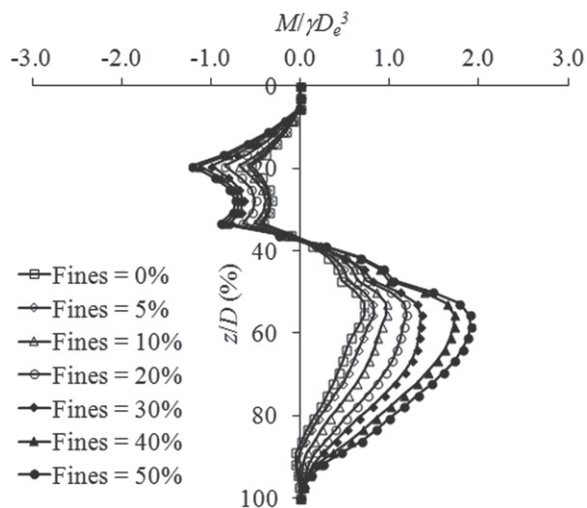


Fig. 8. Comparison of pattern of wall moment when fine content varies from 0 to 50%

Effect of Fines on Wall Deflection

The distribution pattern of normalized wall deflection along the normalized depth of the wall as obtained from numerical analysis of prototype structure for $D_b/D_e = 80\%$, $t_{wall}/D_e = 6\%$, and $k_{strut} = 5 \times 10^5$ kN/m/m, when fine content varies from 0 to 50%, is shown in Fig. 9. The values of the deflection of the wall (u) at different depths below ground level are normalized with respect to D_e , and the normalized deflection is obtained as $u^* = u/D_e$. The depth, z , below ground level is normalized with respect to total depth of the wall, D . Fig. 9 shows that nature of wall deflection along the depth of the wall and the location of maximum wall deflection are similar for different fine contents. Furthermore, it has been observed that the maximum deflection occurs at the final excavation level for all fine contents, and the bulging of the wall becomes predominant as fine content increases from 0 to 50%. The variations of normalized maximum wall deflection (expressed in percentage) with different fine contents are presented in Table 13 when D_b/D_e varies from 60 to 120%, t_{wall}/D_e varies from 4 to 10%, and k_{strut} varies from 1×10^5 – 125×10^5 kN/m/m. It is observed from Table 13 that for a particular value of D_b/D_e , t_{wall}/D_e , and k_{strut} , the value of u^* increases with an increase in fine content, but beyond fine content of 40%, the rate of increment of u^* decreases. This is due to the fact that with the increases in fine content, interface normal and shear

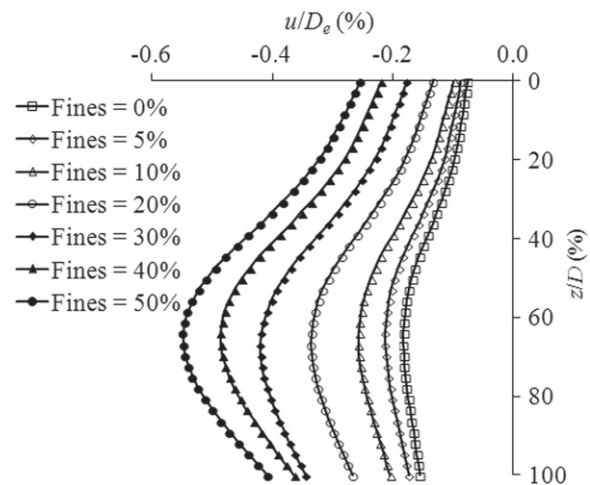


Fig. 9. Comparison of pattern of wall deflection when fine content varies from 0 to 50%

Table 12. Effect of Fines on Normalized Wall Moment (M^*) when D_b/D_e , t_{wall}/D_e , and k_{strut} Vary from 60 to 120%, 4 to 10%, and 1×10^5 to 125×10^5 kN/m/m, Respectively

D_b/D_e (%)	t_{wall}/D_e (%)	$k_{strut} \times 10^5$ kN/m/m	$M^* = M/\gamma D_e^3$ (%)							
			Fines (%)							
			0	5	10	20	30	40	50	
60	6	5	0.725	0.832	0.974	1.167	1.296	1.639	1.773	
80	6	5	0.715	0.828	0.984	1.209	1.372	1.748	1.926	
100	6	5	0.718	0.832	0.980	1.213	1.393	1.753	1.951	
120	6	5	0.720	0.837	0.982	1.209	1.391	1.753	1.911	
80	4	5	0.459	0.522	0.611	0.744	0.852	1.070	1.175	
80	6	5	0.715	0.828	0.984	1.209	1.372	1.748	1.926	
80	8	5	0.972	1.136	1.377	1.733	1.955	2.505	2.763	
80	10	5	1.223	1.391	1.748	2.136	2.416	3.041	3.326	
80	6	1	0.902	1.026	1.223	1.495	1.702	2.136	2.338	
80	6	5	0.715	0.828	0.984	1.209	1.372	1.748	1.926	
80	6	25	0.692	0.791	0.934	1.155	1.354	1.672	1.854	
80	6	125	0.824	0.903	1.068	1.277	1.485	1.795	1.956	

stiffness of the interface element between wall and soil decreases as bulk modulus and shear modulus of the soil also decreases. The cohesion of the soil, interface cohesion increase and friction angle of the soil, and friction angle between the wall and soil decrease with the increase of fine content. The overall combination of all these factors tends to increase the strut force, wall moment, and wall deflection when fine content increases.

It can be also found from Table 13 that the minimum and maximum variations of u^* are 192% (for $D_b/D_e = 120\%$, $t_{wall}/D_e = 6\%$, and $k_{strut} = 5 \times 10^5$ kN/m/m) and 220% (for $D_b/D_e = 80\%$, $t_{wall}/D_e = 4\%$, and $k_{strut} = 5 \times 10^5$ kN/m/m) when fine content varies from 0 to 50%. The lateral wall deflection decreases because of the increase in wall thickness and strut stiffness. If t_{wall}/D_e changes from 6 to 8%, the rate of decrement of normalized lateral deflection of wall increases from 36 to 44% owing to the variation of fine content from 0 to 50%. When k_{strut} varies from 5×10^5 to 25×10^5 kN/m/m, the rate of decrement of normalized lateral deflection of the wall diminishes from 5 to 3% when fine content increases from 0 to 50%. Thus, the wall deflection decreases due because of the increase in thickness of the wall, and the rate of decrease increases because of the addition of fines. Again the wall deflection decreases owing to an increase in strut stiffness, and the rate of decrement decreases because of the addition of fines. However, for any percentage of fines, the reduction of wall deflection is not significant beyond the strut stiffness value of 25×10^5 kN/m/m.

Effect of Fines on Ground Surface Displacement

The variation of normalized ground surface displacement with normalized distance from the wall when fine contents vary from 0 to 50% in the retained soil for $D_b/D_e = 80\%$, $t_{wall}/D_e = 6\%$, and $k_{strut} = 5 \times 10^5$ kN/m/m is shown in Fig. 10. It is found from Fig. 10 that when there is no fine present in the retained soil, heaving is occurring. However, with the increase in fine content, the heaving gradually reduces to settlement. In Fig. 10, the ground surface displacement (v) is normalized with respect to maximum depth of excavation, i.e., D_e , and the normalized ground surface displacement is given by $v^* = v/D_e$; the distance from the wall, x , is normalized with respect to the total depth of the wall, D . The variation of maximum ground surface displacement normalized with respect to D_e (expressed in percentage) with different fine contents is presented in Table 14 when D_b/D_e varies from 60 to 120%, t_{wall}/D_e varies from 4 to 10%, and k_{strut} varies from 1×10^5 to 125×10^5 kN/m/m. It can be found that the maximum variation of v^* is around 150% when fine content varies from 0 to

50%. Moreover, it is also observed that for a particular value of D_b/D_e , t_{wall}/D_e , and k_{strut} , the value of v^* increases with (or almost remains the same as) the increase in fine content up to 30%, beyond which it decreases. Moreover, for a particular fine content, the value of v^* remains almost constant when D_b/D_e varies from 60 to 120%. However, for a particular fine content, the value of v^* decreases with increase in t_{wall}/D_e . Furthermore, for a particular fine content, the value of v^* decreases with increase in strut stiffness up to 25×10^5 kN/m/m and beyond which it again increases. It can be also found from Table 14 that when t_{wall}/D_e changes from 8 to 10%, the rate of decrement of normalized ground surface displacement increases from 24 to 28% when fine content changes from 0 to 30%, beyond which the rate of decrement decreases. When k_{strut} varies from 5×10^5 to 25×10^5 kN/m/m, the rate of decrement of the normalized ground surface displacement increases from 33 to 42% when fine content increases from 0 to 30%, beyond which the rate of decrement again decreases. Thus, ground settlement decreases owing to the increase in wall thickness and strut stiffness, but the rate of decrement increases owing to addition of fines up to 30%; beyond that, it starts decreasing.

Effect of Fines on Net Soil Pressure

For $D_b/D_e = 80\%$, $t_{wall}/D_e = 6\%$, and $k_{strut} = 5 \times 10^5$ kN/m/m, the variation of net soil pressure along the normalized depth of the

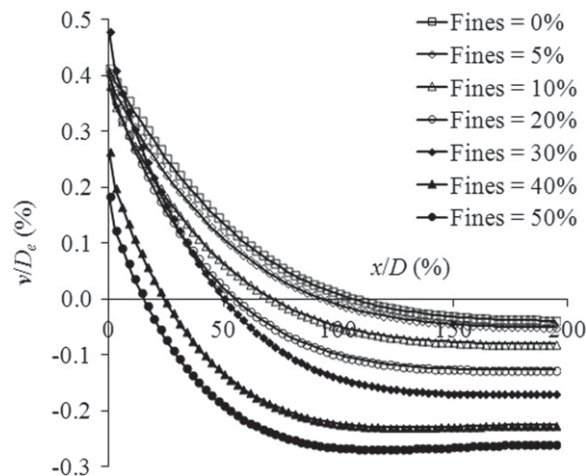


Fig. 10. Comparison of pattern of ground surface displacement when fine content varies from 0 to 50%

Table 13. Effect of Fines on Normalized Wall Deflection u^* when D_b/D_e , t_{wall}/D_e , and k_{strut} Vary from 60 to 120%, 4 to 10%, and 1×10^5 to 125×10^5 kN/m/m, Respectively

D_b/D_e (%)	t_{wall}/D_e (%)	$k_{strut} \times 10^5$ kN/m/m	$u^* = u/D_e$ (%)						
			Fines (%)						
			0	5	10	20	30	40	50
60	6	5	0.181	0.212	0.258	0.339	0.429	0.495	0.563
80	6	5	0.182	0.212	0.257	0.336	0.419	0.486	0.548
100	6	5	0.183	0.213	0.257	0.336	0.420	0.487	0.550
120	6	5	0.184	0.214	0.258	0.337	0.421	0.489	0.537
80	4	5	0.202	0.239	0.289	0.381	0.481	0.568	0.647
80	6	5	0.182	0.212	0.257	0.336	0.419	0.486	0.548
80	8	5	0.167	0.194	0.234	0.305	0.381	0.436	0.492
80	10	5	0.157	0.183	0.221	0.290	0.369	0.412	0.466
80	6	1	0.207	0.239	0.289	0.375	0.466	0.545	0.615
80	6	5	0.182	0.212	0.257	0.336	0.419	0.486	0.548
80	6	25	0.173	0.202	0.246	0.323	0.404	0.468	0.530
80	6	125	0.169	0.198	0.243	0.320	0.401	0.474	0.537

Table 14. Effect of Fines on Normalized Ground Surface Displacement (v^*) when D_b/D_e , t_{wall}/D_e , and k_{strut} Vary from 60 to 120%, 4 to 10%, and 1×10^5 to 125×10^5 kN/m/m, Respectively

D_b/D_e (%)	t_{wall}/D_e (%)	$k_{strut} \times 10^5$ kN/m/m	$v^* = v/D_e$ (%)						
			Fines (%)						
			0	5	10	20	30	40	50
60	6	5	0.402	0.394	0.379	0.395	0.468	0.249	0.268
80	6	5	0.412	0.398	0.382	0.405	0.479	0.264	0.269
100	6	5	0.413	0.388	0.387	0.409	0.478	0.274	0.269
120	6	5	0.404	0.378	0.382	0.406	0.470	0.278	0.272
80	4	5	0.426	0.439	0.425	0.451	0.533	0.318	0.288
80	6	5	0.412	0.398	0.382	0.405	0.479	0.264	0.269
80	8	5	0.361	0.329	0.322	0.331	0.389	0.219	0.255
80	10	5	0.274	0.238	0.241	0.244	0.279	0.210	0.243
80	6	1	0.451	0.430	0.413	0.437	0.513	0.297	0.290
80	6	5	0.412	0.398	0.382	0.405	0.479	0.264	0.269
80	6	25	0.277	0.248	0.245	0.244	0.276	0.210	0.248
80	6	125	0.517	0.413	0.504	0.597	0.757	0.684	0.701

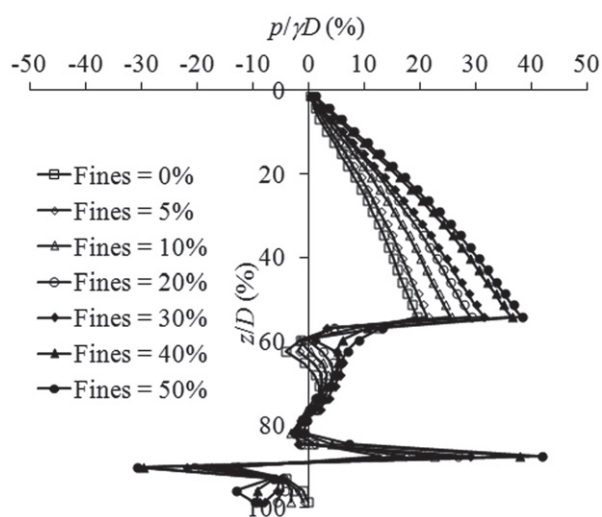


Fig. 11. Comparison of pattern of net pressure distribution on wall when fine content varies from 0 to 50%

wall for different fine contents is shown in Fig. 11. It is found from Fig. 11 that value of maximum normalized net soil pressure increases with increase in fine content. It is concluded from Fig. 11 that patterns of net soil pressure distribution along the depth of the wall and the location of maximum net soil pressure are similar for different fine contents. The maximum net soil pressure is located at the final excavation depth.

On the basis of the results obtained from the model tests on a braced underground structure retaining three types of soil, i.e., pure sand, sand with 5% fines, and sand with 10% fines, it is observed that all four design factors, i.e., strut force, wall moment, wall deflection, and ground surface displacement, are maximum when there is no fine content. These factors decrease when fine content increases from 0 to 5%; however, they increase again when fine content increases from 5 to 10%. Similar results also obtained from numerical modeling of the same model braced underground structure with the same types of soils. However, from the parametric study (on the prototype structure), retaining soil in which fine content varies from 0 to 50%, it is found that the values of all the design factors increase with increase in fine content. The difference between the pattern of variation of the design factors as obtained from small scale physical model and prototype structure

may be due to the fact that the overall behavior of the strutted underground retaining structure depends on many factors, such as geometry of excavation (width and depth), properties of the wall (geometric, i.e., thickness, and embedment depth below final excavation level and material, i.e., modulus of elasticity, Poisson's ratio, density), strut arrangement (position of struts below ground level), properties of the struts (geometric, i.e., cross-sectional area, length, horizontal spacing and material, i.e., modulus of elasticity, Poisson's ratio, density). Furthermore, the construction sequence affects the values of the design factors significantly. The number of struts in the chosen structure for the model study and the parametric study is not the same. In the model study, only one level of strut is used to get measurable deformation of the wall during the experiment [the same as in Nakai et al. (1999) and Tefera et al. (2006)], whereas in the parametric study, four-level struts are chosen. In the model study, the distance of the strut from the top or from the excavation level is higher than the distance of the first strut from the top or distance of the fourth-level strut from the excavation level chosen during the parametric study. Thus, the clear spacing of the strut in the model study is greater than the clear spacing used in the parametric study to get a measurable value of the wall deformation and other design factors. In the present study, the developed numerical model is validated with the experimental results, and later this numerical model is used to do a parametric study of the prototype structure used in the field per the design guidelines proposed by Chowdhury et al. (2013).

Conclusions

From the parametric study of the prototype structure, which has been done by numerical modeling using the same water content and unit weight of the soil, it can be concluded that the pattern of distribution of the wall moment, wall deflection, and net soil pressure along the depth of the wall remains similar for different fine contents. It is also found that for a particular value of D_b/D_e , t_{wall}/D_e , and k_{strut} , maximum strut force, wall moment, and wall deflection increase with the increase in fine content, but the rate of increment decreases beyond fine content of 40%. However, for a particular value of D_b/D_e , t_{wall}/D_e , and k_{strut} the value of ground displacement increases with (or remains almost the same as) the increase in fine content up to 30%, beyond which it decreases. Moreover, the predominant ground surface displacement gradually shifts from heaving to settlement as the fine content in the retained soil increases from

0 to 50%. Thus, it can be concluded that as the soil becomes more cohesive in nature, the values of all the design factors including net soil pressure also increase, and the design has to be done accordingly. The strut force increases owing to the increase in the depth of the embedment and stiffness of the strut. However, the rate of increment decreases because of the increase in fines. For any fine content, the bending moment is lowest when the strut stiffness is kept between $(5-25) \times 10^5$ kN/m/m. The wall moment increases owing to the increase in the thickness of the wall, and the rate of increment increases owing to the addition of fines. The wall deflection decreases owing to the increase of thickness of the wall, and the rate of decrease increases owing to the addition of fines in the soil. The wall deflection also decreases owing to the increases of strut stiffness, but the rate of decrement decreases due to the addition of fines in the soil. However, for any percentage of fines, the reduction of wall deflection is not significant beyond the strut stiffness value of 25×10^5 kN/m/m. It has been further observed that the bulging of the wall becomes predominant as fine content of the fill increases from 0 to 50%. The ground settlement decreases owing to the increase in wall thickness and strut stiffness. However, the rate of decrement increases owing to addition of fines up to 30%; beyond that, the rate of decrement decreases. For a particular fine content, the value of ground displacement decreases with increase in the strut stiffness up to 25×10^5 kN/m/m, beyond which it again increases. The maximum wall deflection and the maximum net soil pressure are located at the final excavation depth. The present study has been conducted for one type of sand and fine with constant unit weight at particular water content. It is also observed that the overall behavior of a strutted underground retaining structure depends on many factors, such as geometry of excavation, strut arrangement, and its properties. Thus, more studies are required to get more generalized conclusions.

Acknowledgments

The financial support for the present work received from the Science and Engineering Research Board (SERB) of the Department of Science and Technology, Government of India, New Delhi is hereby gratefully acknowledged.

Notation

The following symbols are used in this paper:

- A_{strut} = cross-sectional area of the strut;
- B = width of excavation;
- B' = half-width of excavation;
- c = cohesion of soil;
- c_a = adhesion between soil and wall;
- D = depth of the wall;
- D_e = excavation depth (final stage);
- D_b = embedment depth (final stage);
- E_i = modulus of elasticity of soil;
- E_{strut} = modulus of elasticity of the strut material;
- E_{wall} = modulus of elasticity of the wall material;
- F = axial force in the strut;
- F^* = nondimensional axial force in the strut;
- h = spacing of strut from the final excavation level;
- I_{wall} = moment of inertia of the wall;
- K = modulus number;
- K_n = interface normal stiffness between soil and wall;
- K_o = coefficient of lateral earth pressure at rest;
- K_s = interface shear stiffness between soil and wall;

- k_{strut} = strut or support member stiffness;
- k_{wall} = wall stiffness;
- l = length of strut or support member;
- M = bending moment in the wall;
- M^* = nondimensional bending moment in the wall;
- n = modulus exponent;
- P_a = atmospheric pressure;
- p = net soil pressure acting on the wall;
- p^* = normalized net soil pressure;
- s = horizontal spacing of strut or support members;
- t_{wall} = thickness of the wall;
- u = maximum horizontal wall movement;
- u^* = nondimensional horizontal wall movement;
- v = maximum vertical ground surface displacement;
- v^* = nondimensional vertical ground surface displacement;
- x = distance from the retaining wall;
- y = distance between toe of the wall and the bottom of the model tank;
- γ = bulk unit weight of soil;
- Δz_{min} = smallest width of an adjoining zone in the normal direction to the interface;
- δ = wall friction angle;
- ϵ = strain recorded by strain gauges;
- μ = Poisson's ratio of soil;
- μ_{wall} = Poisson's ratio of wall;
- ρ = density of soil;
- σ_3 = confining pressure; and
- ϕ = friction angle of soil under plane-strain condition.

References

- Bose, S. K., and Som, N. N. (1998). "Parametric study of a braced cut by finite element method." *Comput. Geotech.*, 22(2), 91–107.
- Bryson, L. S., and Zapata-Medina, D. G. (2007). "Physical modelling of supported excavations." *Advances in Measurement and Modeling of Soil Behavior*, Geotechnical special publication 117, D. J. DeGroot, C. Vipulanandan, J. A. Yamamuro, V. N. Kaliakin, P. V. Lade, M. Zeghal, U. El Shamy, N. Lu, and C. R. Song, eds., ASCE, Reston, VA, 1–9.
- Chowdhury, S. S., Deb, K., and Sengupta, A. (2013). "Estimation of design parameters for braced excavation: A numerical study." *Int. J. Geomech.*, 10.1061/(ASCE)GM.1943-5622.0000207, 234–247.
- Clough, G. W., and Hansen, L. A. (1981). "Clay anisotropy and braced wall behavior." *J. Geotech. Engrg. Div.*, 107(7), 893–913.
- Costa, P. A., Borges, J. L., Fernandes, M. M. (2007). "Analysis of a braced excavation in soft soils considering the consolidation effect." *J. Geotech. Geol. Eng.*, 25(6), 617–629.
- Grande, L. (1998). "Some aspects on sheet pile wall analysis." *Soil Struct. Interact. Darmstadt*, 1(4), 93–211.
- Hashash, Y. M. A., and Whittle, A. J. (1996). "Ground movement prediction for deep excavation in soft clay." *J. Geotech. Eng.*, 10.1061/(ASCE)0733-9410(1996)122:6(474), 474–486.
- Hashash, Y. M. A., and Whittle, A. J. (2002). "Mechanisms of load transfer and arching for braced excavations in clay." *J. Geotech. Geoenviron. Eng.*, 10.1061/(ASCE)1090-0241(2002)128:3(187), 187–197.
- Hatami, K., and Bathurst, R. J. (2005). "Development and verification of a numerical model for the analysis of geosynthetic-reinforced soil segmental walls under working stress conditions." *Can. Geotech. J.*, 42(4), 1066–1085.
- Hatami, K., and Bathurst, R. J. (2006). "Numerical model for reinforced soil segmental walls under surcharge loading." *J. Geotech. Geoenviron. Eng.*, 10.1061/(ASCE)1090-0241(2006)132:6(673), 673–684.

- Hsiung, B. C. B. (2009). "A case study of behavior of deep excavation in sand." *Comput. Geotech.*, 36(4), 665–675.
- Itasca. (2005). User's guide for *FLAC* version 5.0, Itasca India Consulting, Nagpur, India.
- Janbu, N. (1963). "Soil compressibility as determined by odometer and triaxial tests." *Proc., European Conf. on Soil Mech. and Found. Eng.*, Vol. 1, Wiesbaden, Germany, 19–25.
- Karlsrud, K., and Andresen, L. (2005). "Loads on braced excavations in soft clay." *Int. J. Geomech.*, 10.1061/(ASCE)1532-3641(2005)5:2(107), 107–113.
- Kung, G. T. C. (2009). "Comparison of excavation-induced wall deflection using top-down and bottom-up construction methods in Taipei silty clay." *Comput. Geotech.*, 36(3), 373–385.
- Nakai, T., Hiromichi, K., Murata, K., Banno, M., and Tadashi, H. (1999). "Model tests and numerical simulation of braced excavation in sandy ground: Influences of construction history, wall friction, wall stiffness, strut position and strut stiffness." *Soils Found.*, 39(3), 1–12.
- Ng, C. W. W., and Lings, M. L. (1995). "Effects of modeling soil non-linearity and wall installation on back-analysis of deep excavation in stiff clay." *J. Geotech. Geoenviron. Eng.*, 10.1061/(ASCE)0733-9410(1995)121:10(687), 687–695.
- Takemura, J., Kondoh, M., Esaki, T., Kouda, M., and Kusakabe, O. (1999). "Centrifuge model tests on doubly propped wall excavation in soft clay." *Soils Found.*, 39(3), 75–87.
- Tefera, T. H., Nordal, S., Grande, L., Sandven, R., and Emdal, A. (2006). "Ground settlement and wall deformation from a large scale model test on a single strutted sheet pile wall in sand." *Int. J. Phys. Numer. Modell. Geotech.*, 6(2), 1–13.
- Vaziri, H. H. (1996). "Numerical study of parameters influencing the response of flexible retaining walls." *Can. Geotech. J.*, 33(2), 290–308.
- Wroth, C. P. (1984). "The interpretation of in situ soil tests – Twenty fourth Rankine lecture." *Géotechnique*, 34(4), 449–489.